Theoretical Stability of Ice Shelf Basal Crevasses with a Vertical Temperature Profile

N. B. Coffey[1,2], C. Y. Lai[1,2,3], Y. Wang[3], W. R. Buck[4], T. Surawy-Stepney[5], A. E. Hogg[5]

[1]Department of Geophysics, Stanford University, Stanford, CA, USA
[2]Program in Atmospheric and Oceanic Sciences, Princeton University, Princeton, NJ, USA
[3]Department of Geosciences, Princeton University, Princeton, NJ, USA
[4]Lamont-Doherty Earth Observatory of Columbia University, New York, NY, USA
[5]School of Earth and Environment, University of Leeds, Leeds, UK

Key Points:

- The effect of vertical temperature structure on the stability of ice shelf basal crevasses varies across several theories.
- Rift formation in each theory depends on dimensionless measures of crack depth, density, ice hardness, and resistive stress.
- Rift formation requires a glaciological stress state near that of a freely-floating ice tongue.

Corresponding author: Niall Coffey, `nbcoffey@stanford.edu`

Abstract

Basal crevasses threaten the stability of ice shelves through the potential to form rifts and calve icebergs. Different existing fracture theories lead to distinct calving predictions. Furthermore, it is important to determine the dependence of crevasse stability on temperature due to large vertical temperature variations on ice shelves. In this work, we explore the transition from basal crevasses to full thickness fractures considering the vertical temperature structure. Nye's Zero-Stress approximation violates Newton's second law. By upholding horizontal force balance, it has been shown analytically that the threshold stress for rift initiation is that of a freely- floating unconfined ice tongue. We generalize the force balance argument to show that while temperature structure influences crack depths, the threshold rifting stress is insensitive to temperature. In the classical Nye's theory, basal crevasses would develop into rifts at a stress twice of that in our Nye's theory adhering to horizontal force balance.

Plain Language Summary

Ice shelves, the floating extensions of grounded ice sheets, have the ability to slow down the flow of grounded ice and thus potentially decrease the rate of sea level rise. However, large fractures can damage ice shelves and reduce their ability to slow down sea level rise. In this paper, we focus on large fractures on the bottom surface of ice shelves known as basal crevasses, and under what conditions they break through the full ice thickness to form so-called rifts. We study the role of how a linear temperature profile in the vertical direction modifies existing fracture theories, with specific focus on what stress values lead to rifts. We find that including vertical temperature variations can significantly alter the transition from basal crevasses to rifts among two existing theories, with negligible temperature dependence in a recent extension of the simpler theory. Given the observations of this study, the most accurate theory for predicting rifts has a stress threshold of an unconfined ice tongue, highlighting the sensitivity of ice shelves and importance of ice shelf buttressing. Future work testing the sensitivities of rift formation stress thresholds will help produce more accurate predictions of ice loss and sea level rise.

1 Introduction

Ice shelf buttressing plays an important role in reducing the rate of sea level rise. A reduction in buttressing through calving or other processes can increase the mass loss from ice sheets by increasing the grounding line flux (Thomas & MacAyeal, 1982; Rott et al., 2002; Rignot et al., 2004; Dupont & Alley, 2005; Pritchard et al., 2012; Haseloff & Sergienko, 2018). Basal crevasses, vertical fractures on the underside of ice, can play an important role in the calving process and thus the stability of ice shelves and marine-terminating glaciers (McGrath, Steffen, Rajaram, et al., 2012; Colgan et al., 2016; Jeong et al., 2016). Individual basal crevasses can induce surface crevasses, create surface depressions when sufficiently deep that may enable surface meltwater ponding, reduce the ability of ice shelves to provide back stress to upstream grounded ice, and may penetrate through the full ice thickness to form rifts (McGrath, Steffen, Scambos, et al., 2012; Luckman et al., 2012; Child et al., 2021; Pralong & Funk, 2005). When spaced periodically, basal crevasses can potentially stabilize ice shelves from breakup through dampening stresses transmitted through high-frequency elastic-flexural waves (Freed-Brown et al., 2012). The evolution of basal crevasses has been modeled by the balance of ice shelf and hydrostatic ocean stresses (Zarrinderakht et al., 2022), as well as idealized ocean dynamics and the mass balance of melting and freezing (Jordan et al., 2014). Basal crevasses may play a central role in the flexure-driven calving of marine-terminating glaciers seen in Greenland and Canada (Wagner et al., 2014; Murray et al., 2015; Wagner et al., 2016; Benn et al., 2017). In Antarctica, basal crevasses may initiate rifts that can propagate across the ice shelf and calve icebergs (Lipovsky, 2020). These icebergs can transport fresh meltwater equatorwards and threaten biodiversity of islands in the Southern Ocean (Huth et al., 2022).

While the calving of icebergs is likely caused by multiple mechanisms, we focus on the transition from basal crevasses. In the absence of ample surface meltwater such as surface melt ponds, basal crevasses are theoretically more vulnerable than surface crevasses to full-thickness penetration and cause rift initiation (Lai et al., 2020). The depth-averaged deviatoric stress formulations of Nye (Nye, 1955), Weertman (Weertman, 1973), and the zero toughness or half-space formulations of Mode I Linear Elastic Fracture Mechanics (LEFM) (van der Veen, 1998) all predict basal crevasses to be about nine times deeper than dry (water-free) surface crevasses. The magnitude of lithostatic stress only decreases as basal crevasses propagate upwards, yet increases as surface crevasses propagate downwards, making the initiation of rifts more likely due to basal crevasses than dry surface crevasses. Thus, we study basal crevasses as the precursors of rifts in the absence of strong atmospheric forcing (Morris & Vaughan, 2003; van Wessem et al., 2023).

Driven by the importance to predict rift initiation on ice shelves, here we extend analytical and numerical models to predict the ice shelf threshold stress R_{xx} for rifts to initiate from basal crevasses. Our fracture models' deviations from standard implementations and validation of Nye's Zero-Yield Stress (Nye, 1955) and Mode I LEFM for basal crevasses (van der Veen, 1998) are summarized below. First, we include the depth variation of the resistive stress due to vertical temperature variation in all theories and compare the results. We chose a linear temperature profile for simplicity and show in Supporting Information S5 the effects of a different temperature structure. Second, we modify Nye's Zero-Stress theory to uphold horizontal force balance and include vertical temperature variations, following a procedure similar to (Buck, 2023) and obtaining a simple analytical result. Third, we shift the focus from crevasse depth prediction to rift formation prediction, analyzing results in terms of stress required for basal crevasses to unstably propagate and initiate rifts or calving events. Fourth, we validate rift formation predictions with an existing rift catalog (Walker et al., 2013) on the Ross Ice Shelf (RIS) and Larsen C Ice Shelf (LCIS). We verified that the deviation in resistive stress between the 1D fracture theory and the 2D Shallow-Shelf Approximation (SSA) (MacAyeal, 1989) is less than 10%, thus ensuring validity of the 1D flow assumption in the regions of interest.

2 Fracture Models of Basal Crevasses with Vertically Varying Ice Temperature

[Figure 1 about here.]

Figure 1 shows the differences between existing isothermal basal crevasse depth prediction theories: the Nye's Zero-Stress approximation, LEFM, and a new model based upon Nye's theory in (Buck, 2023). While these theories differ for a range of crack depths, the largest discrepancy is near the sea level, where basal crevasses can unstably propagate and form rifts. Although the basal crevasse to rift transition is challenging to precisely measure (see Supporting Information S2), Figure 1(c-f) motivates our study of rift initiation associated with basal crevasse vertical propagation. Importantly, ice shelves are not isothermal, and basal crevasse depths are sensitive to the ice shelf vertical temperature structure (Rist et al., 2002; Borstad et al., 2012; Lai et al., 2020). We analyze several fracture models (Nye, 1955; van der Veen, 1998; Buck, 2023) and the stress required to form rifts, considering a vertically linear temperature profile for simplicity. We assume that the base of the ice shelf is held at $T_b = -2^\circ$ C, and take a linear temperature profile up to the surface temperature T_s as predicted by RACMO (van Wessem et al., 2018).

The Nye's Zero-Stress (Nye, 1955) and LEFM (van der Veen, 1998) theories presented in this section share many basic assumptions. As shown in Figure 1(a), given a

2D coordinate system with x as the horizontal dimension and z as the vertical dimension, assuming incompressibility and a stress-free upper surface, we can write the net longitudinal stress σ_n of (van der Veen, 1998) at the approximately vertical basal crevasse interface as

$$\sigma_n(z) = R_{xx}(z) - p_l(z) + p_w(z), \tag{1}$$

where $R_{xx}(z)$, $p_l(z)$, and $p_w(z)$ are the along-flow component of ice shelf resistive stress defined in (Cuffey & Paterson, 2010), lithostatic pressure and hydrostatic water pressure, respectively. We assume that there is negligible vertical shear stress in the ice due to negligible shear stress on the surface and basal boundaries, thus simplifying the along-flow component of resistive stress to twice that of the corresponding deviatoric stress component, $R_{xx}(z) \approx 2\tau_{xx}(z)$. By setting $z = 0$ at the ice shelf base and positive upwards as shown in Figure 1(a), we define the pressure terms as $p_l = \rho_i g (H - z)$ and water pressure $p_w = \rho_w g \max(z_h - z, 0)$, with gravitational acceleration $g = 9.8\text{m/s}^2$, vertically integrated ice density $\rho_i = 917\text{kg/m}^3$ and ice thickness H. The piezometric head $z_h = \frac{\rho_i}{\rho_w} H$ as defined in (Nick et al., 2010) depends on the water density; for this study, we assume constant saltwater density $\rho_w = 1028\text{kg/m}^3$.

The way that we account for vertical temperature structure $T(z)$ is through the ice hardness $B(T)$ in the effective viscosity. Modeling ice as a Non-Newtonian power-law fluid (Glen, 1958), the effective viscosity is,

$$\mu = \frac{B(T)}{2} \dot{\epsilon}_e^{\frac{1}{n}-1} \approx \frac{B(T)}{2} \dot{\epsilon}_{xx}^{\frac{1}{n}-1}, \tag{2}$$

where the effective strain rate $\dot{\epsilon}_e$, i.e. the second invariant of the strain rate tensor $\dot{\epsilon}_{ij}$, is dominated by the along-flow component $\dot{\epsilon}_{xx}$. Thus, the along-flow resistive stress $R_{xx} = 2\tau_{xx} = 4\mu\dot{\epsilon}_{xx}$ can be written as

$$R_{xx} = 2B(T)\, \dot{\epsilon}_{xx}^{\frac{1}{n}}. \tag{3}$$

Based on lab experiments, the Glen's flow law gives $n = 3$ (Glen, 1958), and $B(T)$ (LeB. Hooke, 1981) can be expressed as

$$B(T) = B_0 \exp\left[\frac{T_0}{T} - \frac{C}{(T_r - T)^k}\right], \tag{4}$$

where $B_0 = 2.207\ \text{Pa} \cdot \text{yr}^{\frac{1}{n}}$, $T_0 = 3155$ K, $T_r = 273.39$ K, $k = 1.17$, and $C = 0.16612$ K^k are constants determined from empirical fit (LeB. Hooke, 1981).

2.1 Nye's Zero-Yield Stress

Nye's theory (Nye, 1955) assumes that a crevasse will propagate until infinitesimal crack tip growth would put the net longitudinal stress σ_n at the crack tip into compression. Nye's theory is self-consistent when surface and basal crevasses are both allowed to propagate. As derived in Supporting Information S3, a basal crevasse on a freely-floating ice shelf can unstably propagate to the surface when the resistive stress is above the threshold

$$\frac{\overline{R}_{xx}}{\overline{R}_{xx}^{IT}} \geq 2\frac{\rho_w}{\rho_i}\frac{d_b^*}{H}\frac{\overline{\tilde{B}(T)}}{\tilde{B}\left(T\left(\frac{d_b^*}{H}\right)\right)}. \tag{5}$$

In this equation, the overline $\overline{q}$ represents a depth-averaged value for the variable q. The dimensionless numbers involved are the depth-averaged resistive stress $\overline{R}_{xx}$ relative to the isothermal ice tongue resistive stress $\overline{R}_{xx}^{IT} \equiv \frac{1}{2}\left(1 - \frac{\rho_i}{\rho_w}\right)\rho_i g H$ as derived by (Weertman, 1957); the ratio of densities ρ_w/ρ_i; the unstable basal crevasse depth relative to ice thickness d_b^*/H; the nondimensional ice hardness $\tilde{B}(T) \equiv \frac{B(T)}{B(T(z=0))}$; and the nondimensional ice hardness at the unstable basal crevasse depth $\tilde{B}\left(T\left(\frac{d_b^*}{H}\right)\right)$. Note that when we treat the ice as isothermal, the ice hardness ratio $\overline{\tilde{B}\,(T)}/\tilde{B}\left(T\left(\frac{d_b^*}{H}\right)\right)$ is 1, and the maximum basal crevasse depth is from the base to sea level $\frac{\rho_w}{\rho_i}\frac{d_b^*}{H}=1$, making the right-hand side of equation (5) 2. Thus, under Nye's Zero-Stress theory, a basal crevasse will propagate to the sea level, intersecting a surface crevasse to form a rift in isothermal ice when the depth-averaged resistive stress is twice that of an isothermal ice tongue, as shown in Figure 1(b).

The simplicity of Nye's theory comes with limitations. Nye's original theory does not include stress concentration near crack tips, the material strength of ice, accumulation and melt, nor crevasse-induced stresses. The lack of stress concentration and zero material strength is applicable in the limit of closely-spaced crevasses (De Robin, 1974; Weertman, 1974), where the spacing between crevasses is much less than the individual crevasse depths (Weertman, 1977). Observations indicate basal crevasse spacing to be roughly one to several ice thicknesses (Luckman et al., 2012; McGrath, Steffen, Rajaram, et al., 2012; Lawrence et al., 2023), breaking the densely-spaced crevasses assumption in Nye's theory. Recent extensions of Nye's theory include non-zero material strength (Benn et al., 2007) and accumulation and melting effects (Bassis & Ma, 2015; Huth et al., 2021). In the limit of densely-spaced crevasses with negligible flexural stress, the effects of crevasse-induced stress on crack depth has been included to satisfy a horizontal force balance argument (Buck, 2023). We present an approach to generalize this approximate crevasse-induced stress for vertically varying ice temperature in Section 2.3.

2.2 Linear Elastic Fracture Mechanics

In contrast to the Nye's theory, the Linear Elastic Fracture Mechanics (LEFM) framework applied by (van der Veen, 1998) considers an isolated basal crevasse with stress concentration near the crack tip. LEFM agrees with the analytical approach of including stress concentration near crack tips by Weertman (Weertman, 1973) for small crack depths (Buck & Lai, 2021). Unlike Weertman's infinite thickness assumption (Weertman, 1973), LEFM comes with the advantage of accounting for a prescribed finite thickness (van der Veen, 1998), making it well suited for determining rift initiation stresses. The LEFM rifting threshold $\overline{R}_{xx}^*$ for an isothermal ice shelf with traction-free upper and lower surfaces had been reported by (Zarrinderakht et al., 2022) and (Lai et al., 2020). Building on the work of (van der Veen, 1998; Tada et al., 2000; Lai et al., 2020), we extended the LEFM analysis across a range of surface temperatures applicable to Antarctica and present the rifting threshold $\overline{R}_{xx}^*$ for a vertically varying ice temperature. One of the largest simplifications of this version of LEFM is having stress-free upper and lower surface boundary conditions, thus neglecting the oceanic restoring force associated with the vertical displacement at the ice-ocean boundary (Jiménez & Duddu, 2018; Huth et al., 2021; Zarrinderakht et al., 2022). Future work is needed to account for the oceanic restoring force.

2.3 Nye's Zero-Yield Stress with Horizontal Force Balance

Here, we parameterize the crevasse-induced compressive stress through Nye's framework and an Eulerian control volume approach to describe vertically-varying temperature profiles. Note that the control volume argument is Newton's Second Law, and our assumptions of glaciostatic balance and stress distribution represent the limiting case of a densely-crevassed ice shelf where flexural stresses are negligible. In order to satisfy horizontal force balance (HFB), the extra compressive stresses in the unbroken ligament between the surface and basal crevasse tips, induced by the crevasses themselves, needs to be considered. As in Supporting Information S4, we parameterize this crevasse-induced stress to uphold the zero material strength assumption of Nye's theory, continuity of stress at crack tips (Buck & Lai, 2021), and horizontal force balance (Buck, 2023).

Our fixed control volume has vertical boundaries at the ice shelf surface and base, and horizontal boundaries at the symmetry plane of a basal crevasse, $x = x_c$, and at a nearby downstream location $x = x_c + \Delta x$ with the same ice thickness and temperature profile, as depicted in Figure 1. Taking glaciostatic balance (Lindstrom & MacAyeal, 1987),

$$\partial_z \sigma_{zz} = \rho_i g, \tag{6}$$

we can integrate from a level z to the surface H and solve for pressure as $p \equiv -\sigma_{zz} + \tau_{zz} = \rho_i g \left(H - z\right) + \tau_{zz}$ using a stress-free upper surface boundary condition. From the downstream side of the control volume at $x = x_c + \Delta x$, the ice shelf Cauchy stress can be written as

$$\sigma_{xx}\left(x_c + \Delta x, z\right) \equiv -p + \tau_{xx} = -\rho_i g \left(H - z\right) - \tau_{zz} + \tau_{xx} = -\rho_i g \left(H - z\right) + R_{xx}(z), \tag{7}$$

where 2D incompressibility gives $\tau_{xx} = -\tau_{zz}$. Note that this stress distribution is valid for an uncrevassed location, where there is no basal crevasse-induced flexural stress.

At $x = x_c$ the stress can be written in a piecewise fashion corresponding to a dry surface crevasse of depth d_s ($H - d_s \le z \le H$), a water-filled basal crevasse of depth d_b ($0 \le z \le d_b$), and a solid ice ligament between the two ($d_b \le z \le H - d_s$),

$$\sigma_{xx}\left(x_c, z\right) = \begin{cases} 0, & H - d_s \le z \le H \quad \text{(surface crevasse)} \\ -\rho_i g \left(H - z\right) + cR_{xx}(z), & d_b \le z \le H - d_s \quad \text{(unbroken ice)} \\ -\rho_w g \left(z_h - z\right), & 0 \le z \le d_b \quad \text{(basal crevasse)} \end{cases} \tag{8}$$

Here, $cR_{xx}(z)$ represents the sum of the background resistive stress and the crevasse-induced compressive stress in the unbroken ice ligament. We use a constant multiplier c to uphold the zero strength assumption and enforce horizontal force balance, as adding a constant will impose a non-zero material strength. Investigations of material strength effects and crevasse-induced flexural stresses are subject to future work.

When the crack is stable, the crevasse depth is instantaneously determined by the stress states. This is consistent with Nye's and (van der Veen, 1998)'s basal crevasse LEFM consideration neglecting time-dependent fracture propagation, but is a possible future extension (Lawn, 1993). Due to the horizontal force balance on an Eulerian or fixed control volume, defined with negligible inertial term as

$$0 = \int_0^H \int_{x_c}^{x_c + \Delta x} \left[\partial_x \sigma_{xx} + \partial_z \tau_{zx}\right] \mathrm{d}x \mathrm{d}z, \tag{9}$$

the negligible shear stress on the upper and lower surfaces simplifies equation (9) such that the sum of the horizontal forces per unit width into the page on our control volume is zero,

$$\int_0^H \left[\sigma_{xx}\left(x_c + \Delta x\right) - \sigma_{xx}\left(x_c\right)\right] \mathrm{d}z = 0. \tag{10}$$

Solving for the constant c and finding a relation between surface and basal crack depths will close the system of equations, allowing us to determine crevasse depths given a normalized resistive stress $\overline{R}_{xx}/\overline{R}_{xx}^{IT}$. Following (Buck & Lai, 2021), we use continuity of stress at crack tips, $z = H - d_s$ and $z = d_b$, as a constraint to determine the constant c and then a relation between the crevasse depths. At the tip of the surface crevasse, we have that

$$0 = -\rho_i g d_s + c(R_{xx})|_{z=H-d_s}, \tag{11}$$

which easily resolves the constant as

$$c = \frac{\rho_i g d_s}{(R_{xx})|_{z=H-d_s}}. \tag{12}$$

At the basal crevasse tip, we have that

$$-\rho_i g H + \rho_w g d_b = -\rho_i g \left(H - d_b\right) + \frac{\rho_i g d_s}{(R_{xx})|_{z=H-d_s}} (R_{xx})|_{z=d_b}, \tag{13}$$

which can readily be simplified to a dimensionless relation between basal and surface crack depth,

$$\frac{d_b}{d_s} = \frac{\rho_i}{\rho_w - \rho_i} \frac{B\left(T|_{z=d_b}\right)}{B\left(T|_{z=H-d_s}\right)}. \tag{14}$$

Thus the temperature profile $T(z)$ affects the relative surface to basal crevasse depth through $B\left(T\left(z\right)\right)$, with colder surface temperatures creating larger crevasse depth ratio d_s/d_b.

Having solved for the constant, we may now evaluate the force balance constraint of equation (10) with the stress expressions in equations (7) and (8). Defining the dimensionless variables $\tilde{d}_b = d_b/H$, $\tilde{d}_s = d_s/H$, and $\tilde{z} = z/H$, the dimensionless force balance can be written as

$$\frac{\overline{R}_{xx}}{\overline{R}_{xx}^{IT}} = \frac{\rho_w}{\rho_w - \rho_i}\tilde{d}_s^2 + \frac{\rho_w}{\rho_i}\tilde{d}_b^2 + \frac{\tilde{d}_s}{\frac{1}{2}\left(1 - \frac{\rho_i}{\rho_w}\right)\tilde{B}\left(T|_{\tilde{z}=1-\tilde{d}_s}\right)} \int_{\tilde{d}_b}^{1-\tilde{d}_s} \tilde{B}(T(\tilde{z}))d\tilde{z}. \tag{15}$$

Equations (14) and (15) form a system of two equations with the surface and basal crack depths as the two unknowns, given that $\overline{R}_{xx}/\overline{R}_{xx}^{IT}$ is known. For isothermal ice shelves, ice hardness functions become constants as in equation (S12), and the equation has an analytical solution as presented in equation (S17) (Buck, 2023).

When we include the vertical temperature structure, we compute the ice hardness function given vertical temperature variation numerically. We iterate through temperature profiles and basal crevasse depths to solve for surface crevasse depth through the equation residual of equation (14). Having numerically obtained a relation between $\tilde{d}_b$ and $\tilde{d}_s$, we use these values to solve for $\overline{R}_{xx}/\overline{R}_{xx}^{IT}$ in equation (15). We plot dimensionless basal crack depth as a function of $\overline{R}_{xx}/\overline{R}_{xx}^{IT}$ for the linear vertical temperature case in Figure 2. Importantly, we find that the crevasse to rift transition for cold and warm ice shelf surface temperatures occurs at roughly the same critical stress. Thus, Nye's theory with Horizontal Force Balance can be approximated by a simple analytical rifting criteria that is independent of the vertical temperature structure,

$$\frac{\overline{R}_{xx}^*}{\overline{R}_{xx}^{IT}} = 1. \tag{16}$$

2.4 Comparison between the three fracture models

The comparison between the three fracture models is presented in Figure 2. In order of smallest to largest rifting threshold $\overline{R}_{xx}^*/\overline{R}_{xx}^{IT}$, or highest to lowest vulnerability to rifting, we have LEFM, Nye's with Horizontal Force Balance (HFB), and Nye's original theory for all temperatures analyzed in this study. We note that the influence of temperature is distinct between the three theories; while Nye's with HFB has negligible temperature dependence, colder surface temperatures lower the rifting threshold $\overline{R}_{xx}^*/\overline{R}_{xx}^{IT}$ for Nye's original theory yet increase the rifting threshold for LEFM. However, for Nye's with Horizontal Force Balance in Figure 2b), colder surface temperatures cause a decrease (increase) in basal (surface) crevasse depth, yet leave the rifting threshold stress unchanged. Thus, the effect of temperature on basal crevasse depth and rift initiation depends strongly on the chosen theory.

[Figure 2 about here.]

3 Comparison with Observations

[Figure 3 about here.]

As the three fracture theories predict distinct critical stresses that drive the basal crevasse to rift transition, we evaluate the applicability of each theory by comparison with observed rift locations. We analyze our results in two ways. First, we plot the predicted rift locations on MODIS MOA (Scambos et al., 2007; Haran et al., 2018) compared with the rifts previously mapped by (Walker et al., 2013) (labeled as “true rifts”) on Ross Ice Shelf (RIS) in Figure 3. The goal of these rift formation theories is to maximize the overlap between the predicted and true rifts, colored in green in Figure 3. Because we do not have values of strain rate or surface temperature at the time of rifting, the estimated stress state uses modern surface temperature (van Wessem et al., 2018) and strain rate (Wearing, 2017) values, with limitations discussed in Supporting Information S1. In Figure 3, we see that on the RIS rifts identified by (Walker et al., 2013), Nye’s theory with vertical temperature structure underpredicts known rifts as shaded in blue. Similarly, LEFM with a depth-averaged resistive stress, with analytical result given by (Zarrinderakht et al., 2022), overpredicts rifts into areas they were not observed as shaded in red. However, LEFM with vertical temperature structure and Nye’s theory with Horizontal Force Balance are the most accurate theories for these RIS rifts. Their differences are small enough to warrant more observations to distinguish which theory is most applicable.

[Figure 4 about here.]

Second, we construct a crack stability plot of the critical stress $\overline{R}^{*}_{xx}/\overline{R}^{IT}_{xx}$ for rift formation for each theory as a function of the ice surface temperature T_s, as shown by the curves in Figure 4. Noticeably, surface temperature has a negligible effect on the rifting threshold for the Nye’s theory with Horizontal Force Balance; the rifting stress is that of a freely-floating ice tongue, $\overline{R}^{*}_{xx} = \overline{R}^{IT}_{xx} \equiv \frac{1}{2}\left(1 - \frac{\rho_i}{\rho_w}\right)\rho_i g H$. Comparing the rift formation stress criteria, the depth-averaged Nye’s theory requires a resistive stress 200% that of a freely-floating ice tongue to cause rifts, while the depth-averaged formulation for LEFM as presented by (Zarrinderakht et al., 2022) requires only 74% of that of a freely-floating ice tongue to initiate rifts. It is our goal to constrain this substantial uncertainty in the rift initiation stress threshold of these two classical theories, presented by the dashed lines of Figure 4.

We quantitatively compare the rift criteria with the observed rifts on the RIS in Figure 3 and Larsen C Ice Shelf (LCIS) in Figure S3. We identify the extensional, 1D flow regions excluding the rift locations on the RIS and LCIS in Figure S4, and plot the mean depth-averaged resistive stress and surface temperature across these regions in orange on Figure 4 with one standard deviation of uncertainty due to the variation of resistive stress and surface temperature across these regions. The bulk of the non-rift ice shelf data should lie below the curves in Figure 4. While LEFM with depth-averaged resistive stress may look accurate on Figure 4, the overprediction in red is clear in Figures 3c) and S3c). Additionally, the lack of force balance from classical Nye (1955)’s (dashed blue line) and classical Nye (1955)’s with vertical temperature variation (solid green line) invalidates these predictions on theoretical grounds. This lack of force balance manifests as an underprediction of rifting, as discussed in Supporting Information S1 and demonstrated in Figure S9. Therefore, within the uncertainty of our data as discussed in Supporting Information S5, our results on two ice shelves suggest LEFM and Nye’s with Horizontal Force Balance considering the vertically varying ice temperatures are the most accurate theories for classifying the RIS and LCIS ice shelf data as containing or not containing a rift.

4 Discussion and Conclusions

In this paper, we have determined several rift formation stress criteria as functions of surface temperature for linear temperature profiles. We then use remote-sensing and model output data to determine which theory best predicts observed rifts. We find that

Nye's Zero-Stress with either depth-averaged or vertically-varying resistive stress underpredicts rifts, due in part to the inconsistency that the formulations do not uphold force balance as first argued in (Buck, 2023). On the other hand, we find that LEFM with depth-averaged resistive stress overpredicts rifts. Our result shows that on the RIS and LCIS ice shelves, Nye's theory with Horizontal Force Balance and LEFM with vertically-varying resistive stress are the most accurate theories for correctly predicting rifts and non-rifts. Further distinction between these two theories is inhibited by the number of rifts and uncertainty of current data products used in this study. However, given that buoyancy is expected to stabilize basal crevasses (Zarrinderakht et al., 2022) and is not available analytically for the LEFM models, we expect the rift initiation stress threshold of LEFM models to increase. Thus, we recommend the simple, analytical, temperature-independent formulation of Nye's with HFB's rift initiation threshold $\overline{R}_{xx}^{*}/\overline{R}_{xx}^{IT} = 1$ of equation (16), which is both self-consistent and validated against observed rifts on RIS and LCIS. We find a negligible temperature dependence of this rifting threshold. This result appears robust to the choice of temperature profile, having been confirmed in Supporting Information S5 for a Robin temperature profile (Robin, 1955).

A question may then naturally arise: How can the freely-floating ice tongue stress be sufficient to form rifts, yet we see ice tongues exist in nature? It is important here to draw a distinction between idealized ice tongues and those found in nature: any perturbations to the stress field will influence the stability of real ice tongues. For example, sea ice or ice mélange can stabilize these structures through potentially providing a force buttressing the ice shelf and dampening ocean waves that would otherwise induce ice shelf flexural stress (Vaughan, 1995; Bromirski et al., 2010; Sergienko, 2010, 2013; Hulbe et al., 2016; Massom et al., 2018; Gomez-Fell et al., 2022). Indeed, recent observational work analyzing the eastern Antarctic Peninsula found that 94% of calving occurred during or shortly after the removal of sea ice (Christie et al., 2022).

This idealized study is subject to several limitations. We assume 2D (x, z), incompressible, homogeneous density, elastic modulus, and fracture toughness (Rist et al., 2002) ice shelves with zero across-flow strain rate and zero shear strain rate. These theories do not include local thickness variation, creep closure, sub- and super-buoyant flexure (Benn et al., 2017), ice front bending stresses (Reeh, 1968), grain size dependence of yield stress (Ranganathan et al., 2021), snow accumulation, basal melting (Bassis & Ma, 2015; Buck, 2023), and marine ice accumulation. In taking a constant density, we argue with (van der Veen, 1998; Lai et al., 2020) that variations due to firn and an equation of state for ice (Feistel & Wagner, 2006) are negligible for basal crevasse propagation. To uphold the plane strain assumptions of our fracture theories when comparing with observations, we develop a strain rate criteria in Supporting Information S1 to validate locations where the flow is approximately 1D and Mode I fracture is applicable. In reality, ice shelves can also have their stress states altered due to 3D effects such as shear fractures (van der Veen, 1999) and torque from ocean currents (Gomez-Fell et al., 2022; Huth et al., 2022). The interactions of the ocean, sea ice, mass balance, or other additional stresses may determine the stability of the ice tongues and shelves in nature by modulating the ice shelf stress. Effects such as the hydrographic environment in basal crevasses, crevasse-, tidal-, or tsunami-induced flexural stresses (Walker et al., 2013; Brunt et al., 2011; Bromirski et al., 2017; Gerstoft et al., 2017), viscous creep closure, realistic ice rheology, or the time-dependent evolution of basal crevasses evolving into rifts are neglected. We leave the coupling of these processes to future work.

With higher temporal-resolution strain rate estimates than presented in Figure 1(c), cross-rift altimetry, and/or field-based data of the basal crevasse to rift transition, these rifting stress threshold theories provide a basis for comparison. This study provides a simple analytical rift formation stress threshold that can be coupled with numerical ice-sheet simulations. One application could be to enforce that the vertical principal component of damage becomes one from (Huth et al., 2021) when the stress state is above the rift formation stress threshold. In terms of theory, this study advances the common fracture theories used in glaciology through the incorporation of vertical stress variations due to the temperature dependence of the ice hardness, and the modifications of Nye's theory to properly account for horizontal force balance. An interesting extension would be applying Nye's with HFB to the analysis of the ice shelf necking instability developed by (Bassis & Ma, 2015). The different rifting stress theories coupled with ice shelf simulations can lead to distinct calving predictions. Importantly, the classical Nye's theory would largely under-predict the ice mass loss compared with the Nye's with HFB, and impact the sea level projection over the coming centuries.

Data Availability Statement

Strain rates are calculated with the Antarctic velocity field from MEaSUREs Phase-Based Antarctica Ice Velocity Map, Version 1 (NSIDC-0754), available at `https://nsidc.org/data/nsidc-0754/versions/1`. The Antarctic ice thickness field is from MEaSUREs BedMachine Antarctica, Version 2 (NSIDC-0756), available at `https://nsidc.org/data/nsidc-0756/versions/2`. The RACMO 2.3p2 Antarctic surface temperature data are available from `https://doi.org/10.5281/zenodo.7845736`. The MEaSUREs MODIS Mosaic of Antarctica 2013-2014 (MOA2014) Image Map, Version 1 is available at `https://nsidc.org/data/NSIDC-0730/versions/1`. The ENVEO monthly Antarctic velocity data are available at `https://dx.doi.org/10.5285/00fe090efc58446e8980992a617f632f`.

Author Contribution

N.B.C. and C.-Y.L. conceived the study. N.B.C. led the project, numerical and data analysis, and the preparation of the manuscript. Y.W. and W.R.B. contributed to the model discussions. T.S. and A.E.H. processed the strain rates estimates and SAR images in Figure 1, and wrote the corresponding supplementary section on temporal observation.

Acknowledgments

We acknowledge funding from NSF's Office of Polar Programs through OPP-2235051.

References

Bassis, J., & Ma, Y. (2015). Evolution of basal crevasses links ice shelf stability to ocean forcing. *Earth and Planetary Science Letters*, *409*, 203-211. Retrieved from `https://www.sciencedirect.com/science/article/pii/S0012821X14006840` doi: https://doi.org/10.1016/j.epsl.2014.11.003

Benn, D. I., Hulton, N. R. J., & Mottram, R. H. (2007). 'Calving laws', 'sliding laws' and the stability of tidewater glaciers. *Annals of Glaciology*, *46*, 123–130. Retrieved 2023-04-17, from `https://www.cambridge.org/core/journals/annals-of-glaciology/article/calving-laws-sliding-laws-and-the-stability-of-tidewater-glaciers/2B0D6FD7FBEBAB83BA1F4522F37C5CBF` (Publisher: Cambridge University Press) doi: 10.3189/172756407782871161

Benn, D. I., Åström, J., Zwinger, T., Todd, J., Nick, F. M., Cook, S., … Luckman, A. (2017). Melt-under-cutting and buoyancy-driven calving from tidewater glaciers: new insights from discrete element and continuum model simulations. *Journal of Glaciology*, *63*(240), 691–702. doi: 10.1017/jog.2017.41

Borstad, C. P., Khazendar, A., Larour, E., Morlighem, M., Rignot, E., Schodlok, M. P., & Seroussi, H. (2012). A damage mechanics assessment of the larsen b ice shelf prior to collapse: Toward a physically-based calving law. *Geophysical Research Letters*, *39*(18). Retrieved from `https://`

agupubs.onlinelibrary.wiley.com/doi/abs/10.1029/2012GL053317 doi: https://doi.org/10.1029/2012GL053317

Bromirski, P. D., Chen, Z., Stephen, R. A., Gerstoft, P., Arcas, D., Diez, A., ... Nyblade, A. (2017). Tsunami and infragravity waves impacting antarctic ice shelves. *Journal of Geophysical Research: Oceans*, *122*(7), 5786-5801. Retrieved from https://agupubs.onlinelibrary.wiley.com/doi/abs/10.1002/2017JC012913 doi: https://doi.org/10.1002/2017JC012913

Bromirski, P. D., Sergienko, O. V., & MacAyeal, D. R. (2010). Transoceanic infragravity waves impacting Antarctic ice shelves. *Geophysical Research Letters*, *37*(2). Retrieved 2023-02-27, from https://onlinelibrary.wiley.com/doi/abs/10.1029/2009GL041488 (_eprint: https://onlinelibrary.wiley.com/doi/pdf/10.1029/2009GL041488) doi: 10.1029/2009GL041488

Brunt, K. M., Okal, E. A., & MacAyeal, D. R. (2011). Antarctic ice-shelf calving triggered by the honshu (japan) earthquake and tsunami, march 2011. *Journal of Glaciology*, *57*(205), 785–788. doi: 10.3189/002214311798043681

Buck, W. R. (2023). The role of fresh water in driving ice shelf crevassing, rifting and calving. *Earth and Planetary Science Letters*, *624*, 118444. Retrieved from https://www.sciencedirect.com/science/article/pii/S0012821X23004570 doi: https://doi.org/10.1016/j.epsl.2023.118444

Buck, W. R., & Lai, C.-Y. (2021). Flexural control of basal crevasse opening under ice shelves. *Geophysical Research Letters*, *48*(8), e2021GL093110. Retrieved from https://agupubs.onlinelibrary.wiley.com/doi/abs/10.1029/2021GL093110 (e2021GL093110 2021GL093110) doi: https://doi.org/10.1029/2021GL093110

Child, S. F., Stearns, L. A., van der Veen, C. J., & Elósegui, P. (2021). Basal crevasse formation on byrd glacier, east antarctica, as proxy for past subglacial flooding events. *Geophysical Research Letters*, *48*(15), e2020GL090978. Retrieved from https://agupubs.onlinelibrary.wiley.com/doi/abs/10.1029/2020GL090978 (e2020GL090978 2020GL090978) doi: https://doi.org/10.1029/2020GL090978

Christie, F. D., Benham, T. J., Batchelor, C. L., Rack, W., Montelli, A., & Dowdeswell, J. A. (2022). Antarctic ice-shelf advance driven by anomalous atmospheric and sea-ice circulation. *Nature Geoscience*, *15*(5), 356–362.

Colgan, W., Rajaram, H., Abdalati, W., McCutchan, C., Mottram, R., Moussavi, M. S., & Grigsby, S. (2016). Glacier crevasses: Observations, models, and mass balance implications. *Reviews of Geophysics*, *54*(1), 119-161. Retrieved from https://agupubs.onlinelibrary.wiley.com/doi/abs/10.1002/2015RG000504 doi: https://doi.org/10.1002/2015RG000504

Cuffey, K. M., & Paterson, W. S. B. (2010). *The physics of glaciers.* Academic Press.

De Robin, G. Q. (1974). Depth of water-filled crevasses that are closely spaced. *Journal of Glaciology*, *13*(69), 543–543. doi: 10.3189/S0022143000023285

Dupont, T. K., & Alley, R. B. (2005). Assessment of the importance of ice-shelf buttressing to ice-sheet flow. *Geophysical Research Letters*, *32*(4). Retrieved from https://agupubs.onlinelibrary.wiley.com/doi/abs/10.1029/2004GL022024 doi: https://doi.org/10.1029/2004GL022024

Feistel, R., & Wagner, W. (2006). A new equation of state for h2o ice ih. *Journal of Physical and Chemical Reference Data*, *35*(2), 1021-1047. Retrieved from https://doi.org/10.1063/1.2183324 doi: 10.1063/1.2183324

Freed-Brown, J., Amundson, J. M., MacAyeal, D. R., & Zhang, W. W. (2012). Blocking a wave: frequency band gaps in ice shelves with periodic crevasses. *Annals of Glaciology*, *53*(60), 85–89. Retrieved 2023-02-27, from https://www.cambridge.org/core/journals/annals-of-glaciology/article/blocking-a-wave-frequency-band-gaps-in-ice-shelves-with-periodic

-crevasses/3301ACE8900CFE5D18B2CBC9F1B3B5D1 (Publisher: Cambridge University Press) doi: 10.3189/2012AoG60A120

Gerstoft, P., Bromirski, P., Chen, Z., Stephen, R. A., Aster, R. C., Wiens, D. A., & Nyblade, A. (2017, 05). Tsunami excitation of the Ross Ice Shelf, Antarctica. *The Journal of the Acoustical Society of America*, $141(5_Supplement), 3526-3526. Retrievedfrom$ doi: 10.1121/1.4987434

Glen, J. (1958). The flow law of ice: A discussion of the assumptions made in glacier theory, their experimental foundations and consequences. *IASH Publ*, *47*(171), e183.

Gomez-Fell, R., Rack, W., Purdie, H., & Marsh, O. (2022). Parker ice tongue collapse, antarctica, triggered by loss of stabilizing land-fast sea ice. *Geophysical Research Letters*, *49*(1), e2021GL096156. Retrieved from https://agupubs.onlinelibrary.wiley.com/doi/abs/10.1029/2021GL096156 (e2021GL096156 2021GL096156) doi: https://doi.org/10.1029/2021GL096156

Haran, T., Bohlander, J., Scambos, T., Painter, T., & Fahnestock, M. (2013). *2005, updated 2013. modis mosaic of antarctica 2003-2004 (moa2004) image map, version 1. moa125_r1_hp1.img.gz.* (Boulder, Colorado USA. NASA National Snow and Ice Data Center Distributed Active Archive Center. doi: http://dx.doi.org/10.7265/N5ZK5DM5. Accessed 14/06/2021.)

Haran, T., Klinger, M., Bohlander, J., Fahnestock, M., Painter, T., & Scambos., T. (2018). *Measures modis mosaic of antarctica 2013-2014 (moa2014) image map, version 1.* NASA National Snow and Ice Data Center Distributed Active Archive Center. Retrieved from https://nsidc.org/data/NSIDC-0730/versions/1 doi: 10.5067/RNF17BP824UM

Haseloff, M., & Sergienko, O. V. (2018). The effect of buttressing on grounding line dynamics. *Journal of Glaciology*, *64*(245), 417–431. doi: 10.1017/jog.2018.30

Hulbe, C. L., Klinger, M., Masterson, M., Catania, G., Cruikshank, K., & Bugni, A. (2016, October). Tidal bending and strand cracks at the Kamb Ice Stream grounding line, West Antarctica. *Journal of Glaciology*, *62*(235), 816–824. Retrieved 2023-01-30, from https://www.cambridge.org/core/journals/journal-of-glaciology/article/tidal-bending-and-strand-cracks-at-the-kamb-ice-stream-grounding-line-west-antarctica/5A487CC0B853AE66E42D7214EE5CC04A (Publisher: Cambridge University Press) doi: 10.1017/jog.2016.74

Huth, A., Adcroft, A., Sergienko, O., & Khan, N. (2022). Ocean currents break up a tabular iceberg. *Science Advances*, *8*(42), eabq6974. Retrieved from https://www.science.org/doi/abs/10.1126/sciadv.abq6974 doi: 10.1126/sciadv.abq6974

Huth, A., Duddu, R., & Smith, B. (2021). A Generalized Interpolation Material Point Method for Shallow Ice Shelves. 2: Anisotropic Nonlocal Damage Mechanics and Rift Propagation. *Journal of Advances in Modeling Earth Systems*, *13*(8), e2020MS002292. Retrieved 2023-04-20, from https://onlinelibrary.wiley.com/doi/abs/10.1029/2020MS002292 (_eprint: https://onlinelibrary.wiley.com/doi/pdf/10.1029/2020MS002292) doi: 10.1029/2020MS002292

Jeong, S., Howat, I. M., & Bassis, J. N. (2016). Accelerated ice shelf rifting and retreat at pine island glacier, west antarctica. *Geophysical Research Letters*, *43*(22), 11,720-11,725. Retrieved from https://agupubs.onlinelibrary.wiley.com/doi/abs/10.1002/2016GL071360 doi: https://doi.org/10.1002/2016GL071360

Jiménez, S., & Duddu, R. (2018). On the evaluation of the stress intensity factor in calving models using linear elastic fracture mechanics. *Journal of Glaciology*, *64*(247), 759–770. doi: 10.1017/jog.2018.64

Jordan, J. R., Holland, P. R., Jenkins, A., Piggott, M. D., & Kimura, S. (2014). Modeling ice-ocean interaction in ice-shelf crevasses. *Journal of Geophysical Research: Oceans*, *119*(2), 995-1008. Retrieved from https://agupubs.onlinelibrary.wiley.com/doi/abs/10.1002/2013JC009208 doi: https://doi.org/10.1002/2013JC009208

Joughin, I., Shapero, D., Smith, B., Dutrieux, P., & Barham, M. (2021). Ice-shelf retreat drives recent pine island glacier speedup. *Science Advances*, *7*(24), eabg3080. Retrieved from https://www.science.org/doi/abs/10.1126/sciadv.abg3080 doi: 10.1126/sciadv.abg3080

Lai, C.-Y., Kingslake, J., Wearing, M. G., Chen, P.-H. C., Gentine, P., Li, H., . . . van Wessem, J. M. (2020). Vulnerability of antarctica's ice shelves to meltwater-driven fracture. *Nature*, *584*, 574-578. doi: https://doi.org/10.1038/s41586-020-2627-8

Lawn, B. (1993). *Fracture of brittle solids* (2nd ed.). Cambridge University Press. doi: 10.1017/CBO9780511623127

Lawrence, J. D., Washam, P. M., Stevens, C., Hulbe, C., Horgan, H. J., Dunbar, G., . . . Schmidt, B. E. (2023, March). Crevasse refreezing and signatures of retreat observed at Kamb Ice Stream grounding zone. *Nature Geoscience*, *16*(3), 238–243. Retrieved from https://doi.org/10.1038/s41561-023-01129-y doi: 10.1038/s41561-023-01129-y

LeB. Hooke, R. (1981). Flow law for polycrystalline ice in glaciers: Comparison of theoretical predictions, laboratory data, and field measurements. *Reviews of Geophysics*, *19*(4), 664-672. Retrieved from https://agupubs.onlinelibrary.wiley.com/doi/abs/10.1029/RG019i004p00664 doi: https://doi.org/10.1029/RG019i004p00664

Lindstrom, D., & MacAyeal, D. (1987). Environmental constraints on west antarctic ice-sheet formation. *Journal of Glaciology*, *33*(115), 346–356. doi: 10.3189/S0022143000008947

Lipovsky, B. P. (2020). Ice shelf rift propagation: stability, three-dimensional effects, and the role of marginal weakening. *The Cryosphere*, *14*(5), 1673–1683. Retrieved from https://tc.copernicus.org/articles/14/1673/2020/ doi: 10.5194/tc-14-1673-2020

Luckman, A., Jansen, D., Kulessa, B., King, E. C., Sammonds, P., & Benn, D. I. (2012). Basal crevasses in larsen c ice shelf and implications for their global abundance. *The Cryosphere*, *6*, 113–123. doi: 10.5194/tc-6-113-2012

MacAyeal, D. R. (1989). Large-scale ice flow over a viscous basal sediment: Theory and application to ice stream b, antarctica. *Journal of Geophysical Research: Solid Earth*, *94*(B4), 4071-4087. Retrieved from https://agupubs.onlinelibrary.wiley.com/doi/abs/10.1029/JB094iB04p04071 doi: https://doi.org/10.1029/JB094iB04p04071

Massom, R. A., Scambos, T. A., Bennetts, L. G., Reid, P., Squire, V. A., & Stammerjohn, S. E. (2018, June). Antarctic ice shelf disintegration triggered by sea ice loss and ocean swell. *Nature*, *558*(7710), 383–389. Retrieved 2023-02-27, from https://www.nature.com/articles/s41586-018-0212-1 (Number: 7710 Publisher: Nature Publishing Group) doi: 10.1038/s41586-018-0212-1

McGrath, D., Steffen, K., Rajaram, H., Scambos, T., Abdalati, W., & Rignot, E. (2012). Basal crevasses on the larsen c ice shelf, antarctica: Implications for meltwater ponding and hydrofracture. *Geophysical Research Letters*, *39*(16). Retrieved from https://agupubs.onlinelibrary.wiley.com/doi/abs/10.1029/2012GL052413 doi: https://doi.org/10.1029/2012GL052413

McGrath, D., Steffen, K., Scambos, T., Rajaram, H., Casassa, G., & Rodriguez Lagos, J. L. (2012). Basal crevasses and associated surface crevassing on the larsen c ice shelf, antarctica, and their role in ice-shelf instability. *Annals of Glaciology*, *53*(60), 10–18. doi: 10.3189/2012AoG60A005

Morris, E. M., & Vaughan, D. G. (2003). Spatial and temporal variation of surface temperature on the antarctic peninsula and the limit of viability of ice shelves. *Antarctic Research Series*, *79*(10.1029).

Mouginot, J., Scheuchl, B., & Rignot, E. (2017). *Measures antarctic boundaries for ipy 2007-2009 from satellite radar, version 2.* (Boulder, Colorado USA. NASA National Snow and Ice Data Center Distributed Active Archive Center. doi: http://dx.doi.org/10.5067/AXE4121732AD. Accessed 10/07/2023.)

Murray, T., Selmes, N., James, T. D., Edwards, S., Martin, I., O'Farrell, T., … Baugé, T. (2015). Dynamics of glacier calving at the ungrounded margin of helheim glacier, southeast greenland. *Journal of Geophysical Research: Earth Surface*, *120*(6), 964-982. Retrieved from https://agupubs.onlinelibrary.wiley.com/doi/abs/10.1002/2015JF003531 doi: https://doi.org/10.1002/2015JF003531

Nick, F., Van Der Veen, C., Vieli, A., & Benn, D. (2010). A physically based calving model applied to marine outlet glaciers and implications for the glacier dynamics. *Journal of Glaciology*, *56*(199), 781–794. doi: 10.3189/002214310794457344

Nye, J. F. (1955). Comments on dr. loewe's letter and notes on crevasses. *Journal of Glaciology*, *2*(17), 512–514. doi: 10.3189/S0022143000032652

Pralong, A., & Funk, M. (2005). Dynamic damage model of crevasse opening and application to glacier calving. *Journal of Geophysical Research: Solid Earth*, *110*(B1). Retrieved from https://agupubs.onlinelibrary.wiley.com/doi/abs/10.1029/2004JB003104 doi: https://doi.org/10.1029/2004JB003104

Pritchard, H., Ligtenberg, S., Fricker, H., Vaughan, D., van den Broeke, M., & Padman, L. (2012). Antarctic ice loss driven by ice-shelf melt. *Nature*, *484*, 502–505.

Ranganathan, M., Minchew, B., Meyer, C. R., & Peč, M. (2021). Recrystallization of ice enhances the creep and vulnerability to fracture of ice shelves. *Earth and Planetary Science Letters*, *576*, 117219. Retrieved from https://www.sciencedirect.com/science/article/pii/S0012821X2100474X doi: https://doi.org/10.1016/j.epsl.2021.117219

Reeh, N. (1968). On the calving of ice from floating glaciers and ice shelves. *Journal of Glaciology*, *7*(50), 215–232. doi: 10.3189/S0022143000031014

Rignot, E., Casassa, G., Gogineni, P., Krabill, W., Rivera, A., & Thomas, R. (2004). Accelerated ice discharge from the antarctic peninsula following the collapse of larsen b ice shelf. *Geophysical Research Letters*, *31*(18). Retrieved from https://agupubs.onlinelibrary.wiley.com/doi/abs/10.1029/2004GL020697 doi: https://doi.org/10.1029/2004GL020697

Rist, M. A., Sammonds, P. R., Oerter, H., & Doake, C. S. M. (2002). Fracture of antarctic shelf ice. *Journal of Geophysical Research: Solid Earth*, *107*(B1), ECV 2-1-ECV 2-13. Retrieved from https://agupubs.onlinelibrary.wiley.com/doi/abs/10.1029/2000JB000058 doi: https://doi.org/10.1029/2000JB000058

Robin, G. d. Q. (1955). Ice movement and temperature distribution in glaciers and ice sheets. *Journal of Glaciology*, *2*(18), 523–532. doi: 10.3189/002214355793702028

Rott, H., Rack, W., Skvarca, P., & Angelis, H. D. (2002). Northern larsen ice shelf, antarctica: further retreat after collapse. *Annals of Glaciology*, *34*, 277–282. doi: 10.3189/172756402781817716

Scambos, T., Haran, T., Fahnestock, M., Painter, T., & Bohlander, J. (2007). Modis-based mosaic of antarctica (moa) data sets: Continent-wide surface morphology and snow grain size. *Remote Sensing of Environment*, *111*(2), 242-257. Retrieved from https://www.sciencedirect.com/science/article/pii/S0034425707002854 (Remote Sensing of the Cryosphere Special Issue) doi: https://doi.org/10.1016/j.rse.2006.12.020

Sergienko, O. V. (2010). Elastic response of floating glacier ice to impact of long-period ocean waves. *Journal of Geophysical Research: Earth Surface*, *115*(F4). Retrieved 2023-01-24, from https://onlinelibrary.wiley.com/doi/abs/10.1029/2010JF001721 (_eprint: https://onlinelibrary.wiley.com/doi/pdf/10.1029/2010JF001721) doi: 10.1029/2010JF001721

Sergienko, O. V. (2013). Normal modes of a coupled ice-shelf/sub-ice-shelf cavity system. *Journal of Glaciology*, *59*(213), 76–80. Retrieved 2023-02-27, from https://www.cambridge.org/core/product/identifier/S0022143000203420/type/journal_article doi: 10.3189/2013JoG12J096

Tada, H., Paris, P. C., & Irwin, G. R. (2000). *The Stress Analysis of Cracks Handbook, Third Edition.* ASME Press. Retrieved from https://doi.org/10.1115/1.801535 doi: 10.1115/1.801535

Thomas, R. H., & MacAyeal, D. R. (1982). Derived characteristics of the ross ice shelf, antarctica. *Journal of Glaciology*, *28*(100), 397–412. doi: 10.3189/S0022143000005025

van der Veen, C. (1998). Fracture mechanics approach to penetration of bottom crevasses on glaciers. *Cold Regions Science and Technology*, *27*(3), 213-223. doi: https://doi.org/10.1016/S0165-232X(98)00006-8

van der Veen, C. J. (1999). Crevasses on glaciers. *Polar Geography*, *23*(3), 213-245. Retrieved from https://doi.org/10.1080/10889379909377677 doi: 10.1080/10889379909377677

van Wessem, J. M., van de Berg, W. J., Noël, B. P. Y., van Meijgaard, E., Amory, C., Birnbaum, G., ... van den Broeke, M. R. (2018). Modelling the climate and surface mass balance of polar ice sheets using racmo2 – part 2: Antarctica (1979–2016). *The Cryosphere*, *12*(4), 1479–1498. Retrieved from https://tc.copernicus.org/articles/12/1479/2018/ doi: 10.5194/tc-12-1479-2018

van Wessem, J. M., van den Broeke, M. R., Wouters, B., & Lhermitte, S. (2023). Variable temperature thresholds of melt pond formation on antarctic ice shelves. *Nature Climate Change*, *13*(2), 161–166.

Vaughan, D. G. (1995). Tidal flexure at ice shelf margins. *Journal of Geophysical Research: Solid Earth*, *100*(B4), 6213-6224. Retrieved from https://agupubs.onlinelibrary.wiley.com/doi/abs/10.1029/94JB02467 doi: https://doi.org/10.1029/94JB02467

Wagner, T. J. W., James, T. D., Murray, T., & Vella, D. (2016). On the role of buoyant flexure in glacier calving. *Geophysical Research Letters*, *43*(1), 232-240A. Retrieved from https://agupubs.onlinelibrary.wiley.com/doi/abs/10.1002/2015GL067247 doi: https://doi.org/10.1002/2015GL067247

Wagner, T. J. W., Wadhams, P., Bates, R., Elosegui, P., Stern, A., Vella, D., ... Nicholls, K. W. (2014). The "footloose" mechanism: Iceberg decay from hydrostatic stresses. *Geophysical Research Letters*, *41*(15), 5522-5529. Retrieved from https://agupubs.onlinelibrary.wiley.com/doi/abs/10.1002/2014GL060832 doi: https://doi.org/10.1002/2014GL060832

Walker, C. C., Bassis, J. N., Fricker, H. A., & Czerwinski, R. J. (2013). Structural and environmental controls on antarctic ice shelf rift propagation inferred from satellite monitoring. *Journal of Geophysical Research: Earth Surface*, *118*(4), 2354-2364. Retrieved from https://agupubs.onlinelibrary.wiley.com/doi/abs/10.1002/2013JF002742 doi: https://doi.org/10.1002/2013JF002742

Wearing, M. G. (2017). The flow dynamics and buttressing of ice shelves phd thesis.

Weertman, J. (1957). Deformation of floating ice shelves. *Journal of Glaciology*, *3*(21), 38–42. doi: 10.3189/S0022143000024710

Weertman, J. (1973). Can a water-filled crevasse reach the bottom surface of a glacier. *IASH publ*, *95*, 139–145.

Weertman, J. (1974). Depth of water-filled crevasses that are closely spaced. *Journal of Glaciology*, *13*(69), 544–544. doi: 10.3189/S0022143000023297

Weertman, J. (1977). Penetration depth of closely spaced water-free crevasses. *Journal of Glaciology*, *18*(78), 37–46. doi: 10.3189/S0022143000021493

Wuite, J., Hetzenecker, M., Nagler, T., & Scheiblauer, S. (2021). *Esa antarctic ice sheet climate change initiative (antarctic_ice_sheet_cci): Antarctic ice sheet monthly velocity from 2017 to 2020, derived from sentinel-1, v1.* NERC EDS Centre for Environmental Data Analysis. Retrieved from https://dx.doi.org/10.5285/00fe090efc58446e8980992a617f632f doi: 10.5285/00fe090efc58446e8980992a617f632f

Zarrinderakht, M., Schoof, C., & Peirce, A. (2022). The effect of hydrology and crevasse wall contact on calving. *The Cryosphere*, *16*(10), 4491–4512. Retrieved from https://tc.copernicus.org/articles/16/4491/2022/ doi: 10.5194/tc-16-4491-2022

References from Supporting Information

Buck, W. R. (2023). The role of fresh water in driving ice shelf crevassing, rifting and calving. *Earth and Planetary Science Letters, 624*, 118444. Retrieved from https://www.sciencedirect.com/science/article/pii/S0012821X23004570 doi: https:// doi.org/10.1016/j.epsl.2023.118444

Chartrand, R. (2017). Numerical differentiation of noisy, nonsmooth, multidimensional data. In *2017 ieee global conference on signal and information processing (globalsip)* (p. 244-248). doi: 10.1109/GlobalSIP.2017.8308641

Craven, M., Allison, I., Fricker, H. A., Warner, R. (2009). Properties of a marine ice layer under the amery ice shelf, east antarctica. *Journal of Glaciology, 55*(192), 717–728. doi: 10.3189/002214309789470941

Fowler, A., Ng, F. (2020). *Glaciers and ice sheets in the climate system: The karthaus summer school lecture notes.* Springer Nature.

Hulbe, C. L., Rignot, E., Macayeal, D. R. (1998). Comparison of ice-shelf creep flow simulations with ice-front motion of filchner-ronne ice shelf, antarctica, detected by sar interferometry. *Annals of Glaciology, 27*, 182–186. doi: 10.3189/1998AoG27-1-182-186

Jeong, S., Howat, I. M., Bassis, J. N. (2016). Accelerated ice shelf rifting and retreat at pine island glacier, west antarctica. *Geophysical Research Letters, 43*(22), 11,720- 11,725. Retrieved from `https://agupubs.onlinelibrary.wiley.com/doi/abs/10.1002/2016GL071360` doi: https://doi.org/10.1002/2016GL071360

Jezek, K. C. (1984). A modified theory of bottom crevasses used as a means for measuring the buttressing effect of ice shelves on inland ice sheets. *Journal of Geophysical Research: Solid Earth, 89*(B3), 1925-1931. Retrieved from `https://agupubs.onlinelibrary.wiley.com/doi/abs/10.1029/JB089iB03p01925` doi: https://doi.org/10.1029/JB089iB03p01925

LeB. Hooke, R. (1981). Flow law for polycrystalline ice in glaciers: Comparison of theoretical predictions, laboratory data, and field measurements. *Reviews of Geophysics, 19*(4), 664-672. Retrieved from `https://agupubs.onlinelibrary.wiley.com/doi/abs/10.1029/RG019i004p00664` doi: https://doi.org/10.1029/RG019i004p00664

MacAyeal, D. R. (1989). Large-scale ice flow over a viscous basal sediment: Theory and application to ice stream b, antarctica. *Journal of Geophysical Research: Solid Earth, 94*(B4), 4071-4087. Retrieved from `https://agupubs.onlinelibrary.wiley.com/doi/abs/10.1029/JB094iB04p04071` doi: https://doi.org/10.1029/JB094iB04p04071

MacAyeal, D. R., Rignot, E., Hulbe, C. L. (1998). Ice-shelf dynamics near the front of the filchner-ronne ice shelf, antaretica, revealed by sar interferometry: model/interferogram comparison. *Journal of Glaciology, 44*(147), 419–428. doi: 10.3189/S0022143000002744

Morlighem, M. (2020). *Measures bedmachine antarctica, version 2.* NASA National Snow and Ice Data Center Distributed Active Archive Center. Retrieved from `https://nsidc.org/data/NSIDC-0756/versions/2` doi: 10.5067/E1QL9HFQ7A8M

Morlighem, M., Rignot, E., Binder, T., Blankenship, D., Drews, R., Eagles, G., . . . others (2020). Deep glacial troughs and stabilizing ridges unveiled beneath the margins of the antarctic ice sheet. *Nature Geoscience, 13*(2), 132–137.

Mouginot, J., Rignot, E., Scheuchl, B., Millan, R. (2017). Comprehensive annual ice sheet velocity mapping using landsat-8, sentinel-1, and radarsat-2 data. *Remote Sensing, 9*(4). Retrieved from `https://www.mdpi.com/2072-4292/9/4/364` doi: 10.3390/rs9040364

Mouginot, J., Scheuchl, B., Rignot, E. (2012). Mapping of ice motion in antarctica using synthetic-aperture radar data. *Remote Sensing, 4*(9), 2753–2767. Retrieved from `https://www.mdpi.com/2072-4292/4/9/2753` doi: 10.3390/rs4092753

Nicholls, K. W., Corr, H. F., Stewart, C. L., Lok, L. B., Brennan, P. V., Vaughan, D. G. (2015). A ground-based radar for measuring vertical strain rates and time-varying basal melt rates in ice sheets and shelves. *Journal of Glaciology, 61*(230), 1079–1087. doi: 10.3189/2015JoG15J073

Nye, J. F. (1955). Comments on dr. loewe's letter and notes on crevasses. *Journal of Glaciology, 2*(17), 512–514. doi: 10.3189/S0022143000032652

Reeh, N. (1968). On the calving of ice from floating glaciers and ice shelves. *Journal of Glaciology, 7*(50), 215–232. doi: 10.3189/S0022143000031014

Rignot, E., MacAyeal, D. R. (1998). Ice-shelf dynamics near the front of the filchner—ronne ice shelf, antarctica, revealed by sar interferometry. *Journal of Glaciology, 44*(147), 405–418. doi: 10.3189/S0022143000002732

Rignot, E., Mouginot, J., Scheuchl, B. (2011). Ice flow of the antarctic ice sheet. *Science, 333*(6048), 1427-1430. Retrieved from https://www.science.org/doi/abs/10.1126/science.1208336 doi: 10.1126/science.1208336

Rignot, E., Mouginot, J., Scheuchl, B. (2017). Measures insar-based antarctica ice velocity map, version 2. NASA National Snow and Ice Data Center Distributed Active Archive Center. Retrieved from https://nsidc.org/data/NSIDC-484/versions/2 doi: 10.5067/D7GK8F5J8M8R

Rist, M. A., Sammonds, P. R., Oerter, H., Doake, C. S. M. (2002). Fracture of antarctic shelf ice. *Journal of Geophysical Research: Solid Earth, 107*(B1), ECV 2-1-ECV 2-13. Retrieved from https://agupubs.onlinelibrary.wiley.com/doi/abs/10.1029/2000JB000058 doi: https://doi.org/10.1029/2000JB000058

Robin, G. d. Q. (1955). Ice movement and temperature distribution in glaciers and ice sheets. *Journal of Glaciology, 2*(18), 523–532. doi: 10.3189/002214355793702028

Sandhäger, H., Rack, W., Jansen, D. (2005). Model investigations of larsen b ice shelf dynamics prior to the breakup. *FRISP Rep, 16*, 5–12.

Sergienko, O. V. (2014). A vertically integrated treatment of ice stream and ice shelf thermodynamics. *Journal of Geophysical Research: Earth Surface, 119*(4), 745-757. Retrieved from https://agupubs.onlinelibrary.wiley.com/doi/abs/10.1002/2013JF002908 doi: https://doi.org/10.1002/2013JF002908

Sergienko, O. V., Goldberg, D. N., Little, C. M. (2013). Alternative ice shelf equilibria determined by ocean environment. *Journal of Geophysical Research: Earth Surface, 118*(2), 970-981. Retrieved from https://agupubs.onlinelibrary.wiley.com/doi/abs/10.1002/jgrf.20054 doi: https://doi.org/10.1002/jgrf.20054

Taylor, J. R. (1982). *An introduction to error analysis: the study of uncertainties in physical measurements* (Vol. 2). Springer.

Thomas, R. H., MacAyeal, D. R. (1982). Derived characteristics of the ross ice shelf, antarctica. *Journal of Glaciology, 28*(100), 397–412. doi: 10.3189/S0022143000005025

Tyler, S., Holland, D., Zagorodnov, V., Stern, A., Sladek, C., Kobs, S., . . . Bryenton, J. (2013). Using distributed temperature sensors to monitor an antarctic ice shelf and sub-ice-shelf cavity. *Journal of Glaciology, 59*(215), 583–591. doi: 10.3189/2013JoG12J207

van den Broeke, M. (2008). Depth and density of the antarctic firn layer. *Arctic, Antarctic, and Alpine Research, 40*(2), 432–438.

van Wessem, J. M., van de Berg, W. J., Noël, B. P. Y., van Meijgaard, E., Amory, C., Birnbaum, G., . . . van den Broeke, M. R. (2018). Modelling the climate and surface mass balance of polar ice sheets using racmo2 – part 2: Antarctica (1979–2016). *The Cryosphere, 12*(4), 1479–1498. Retrieved from https://tc.copernicus.org/articles/12/1479/2018/ doi: 10.5194/tc-12-1479-2018

Wagner, T. J. W., James, T. D., Murray, T., Vella, D. (2016). On the role of buoyant flexure in glacier calving. *Geophysical Research Letters, 43*(1), 232-240A. Retrieved from https://agupubs.onlinelibrary.wiley.com/doi/abs/10.1002/2015GL067247 doi: https://doi.org/10.1002/2015GL067247

Walker, C. C., Bassis, J. N., Fricker, H. A., Czerwinski, R. J. (2013). Structural and environmental controls on antarctic ice shelf rift propagation inferred from satellite monitoring. *Journal of Geophysical Research: Earth Surface, 118*(4), 2354-2364. Retrieved from https://agupubs.onlinelibrary.wiley.com/doi/abs/10.1002/2013JF002742 doi: https://doi.org/10.1002/2013JF002742

Wearing, M. G. (2017). The flow dynamics and buttressing of ice shelves phd thesis.

Weertman, J. (1957). Deformation of floating ice shelves. *Journal of Glaciology, 3*(21), 38–42. doi: 10.3189/S0022143000024710

Wuite, J., Hetzenecker, M., Nagler, T., Scheiblauer, S. (2021). *Esa antarctic ice sheet climate change initiative (antarctic ice sheet cci): Antarctic ice sheet monthly velocity from 2017 to 2020, derived from sentinel-1, v1.* NERC EDS Centre for Environmental Data Analysis. Retrieved from https://dx.doi.org/10.5285/00fe090efc58446e8980992a617f632f doi: 10.5285/00fe090efc58446e8980992a617f632f

Zarrinderakht, M., Schoof, C., Peirce, A. (2022). The effect of hydrology and crevasse wall contact on calving. *The Cryosphere, 16*(10), 4491–4512. Retrieved from https://tc.copernicus.org/articles/16/4491/2022/ doi: 10.5194/tc-16-4491-2022

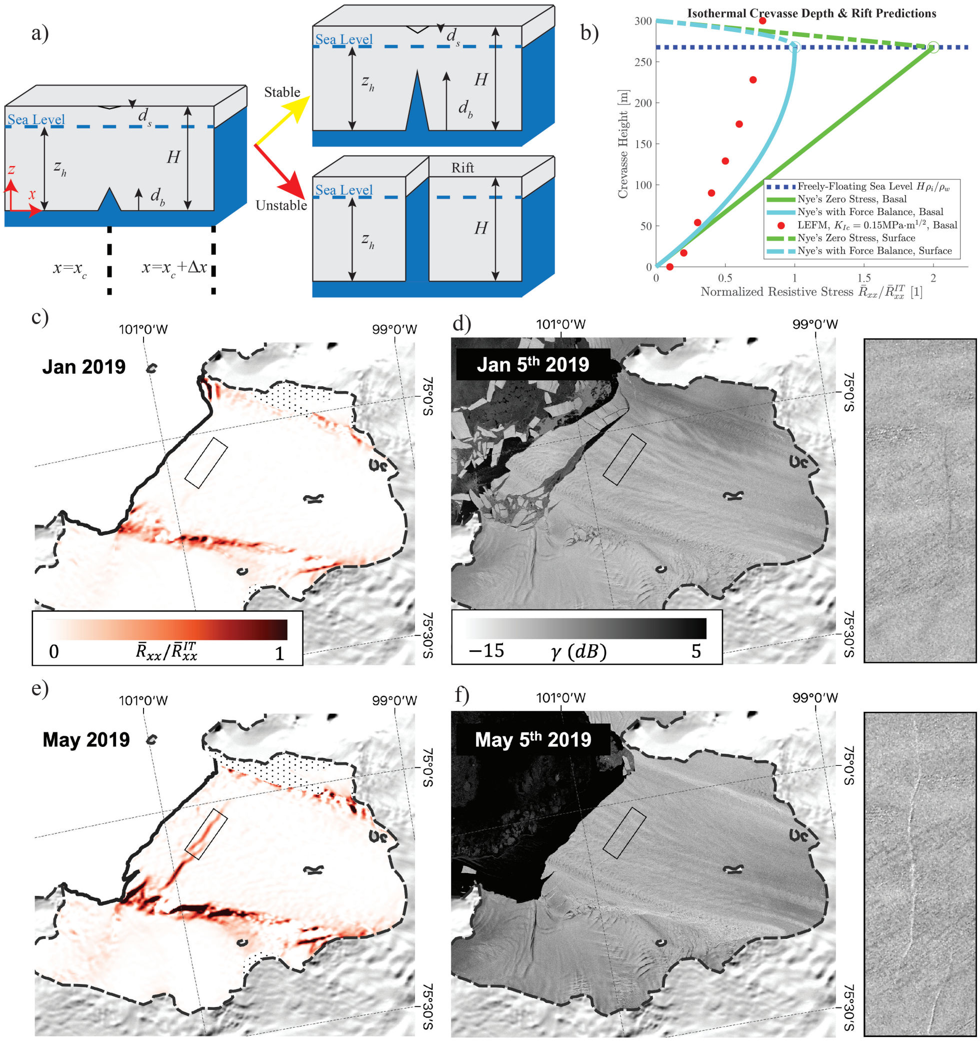

Figure 1. a) Schematic of crevasses propagating stably or unstably and forming a full-thickness fracture called a rift. Crevasse depths d_s, d_b, thickness H, coordinate system, and piezometric head at sea level z_h are illustrated. b) Several previously existing isothermal crevasse depth predictions versus depth-averaged resistive stress $\overline{R}_{xx}$ normalized by the analytical depth-averaged resistive stress $\overline{R}_{xx}^{IT}$ for an unconfined ice tongue with H=300 meters. Circular red dots are LEFM basal crevasse depth numerical predictions, solid lines are basal crevasse depth analytical theory, and dash-dotted lines are surface crevasse depth analytical theory. Rifts initiate either where d_b=H for LEFM or at the open circles that denote the intersection of surface and basal crevasse tips for Nye's Zero-Stress approximation. Formulations based on Nye's theory require surface and basal crevasses for theoretical consistency, whereas LEFM treats an isolated basal crevasse. Subfigures c) to f) show a potential instance of the basal crevasse-to-rift transition (Jeong et al., 2016; Joughin et al., 2021) over Pine Island Ice Shelf during January to May 2019. c) An estimate of the ratio $\overline{R}_{xx}/\overline{R}_{xx}^{IT}$ over Pine Island Ice Shelf in January 2019, found using ice velocity data averaged over the month of January 2019 (Wuite et al., 2021). d) SAR backscatter image at 50m resolution from 5th January 2019, and a close-up showing the terminus region of Pine Island Ice Shelf where a fracture (can be surface crack, surface expression of basal crack or rift) is dimly visible. e) The equivalent of (c) for May 2019. f) A backscatter image from May 2019 where a rift is clearly visible. Grounding lines according to Mouginot et al. (2017) are shown with a dashed black line. Grounded ice is masked with a MODIS Mosaic of Antarctica (Haran et al., 2013). Calving fronts are marked with a black line.

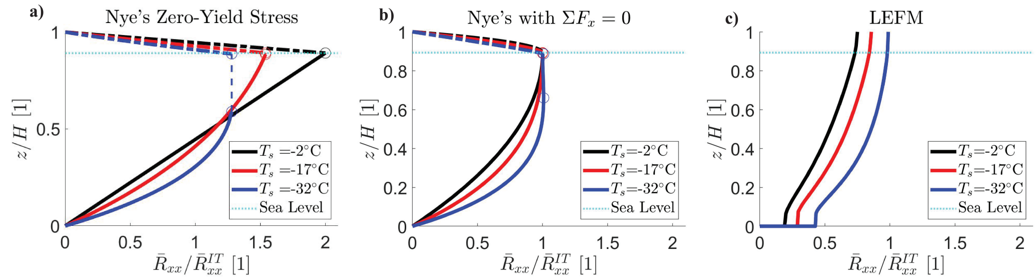

Figure 2. Predicted crevasse depths for a) Nye's theory, b) Nye's with horizontal force balance, and c) linear elastic fracture mechanics given a linear temperature profile in the vertical direction from a basal temperature of $-2°$C to surface temperature T_s. The y-axes are nondimensional height from the ice shelf base, and the x-axes are depth-averaged resistive stress normalized by depth-averaged ice tongue resistive stress. The solid lines are the basal crack depths, the dash-dotted lines are surface crevasse depths, and the vertical dashed lines and circles are where unstable basal crevasses propagate to meet surface crevasses for the given B and linear $T(z)$. The isothermal cases presented here at $T = -2°$C of Nye's and Nye's with Horizontal Force Balance are analytical, while all other results are numerical.

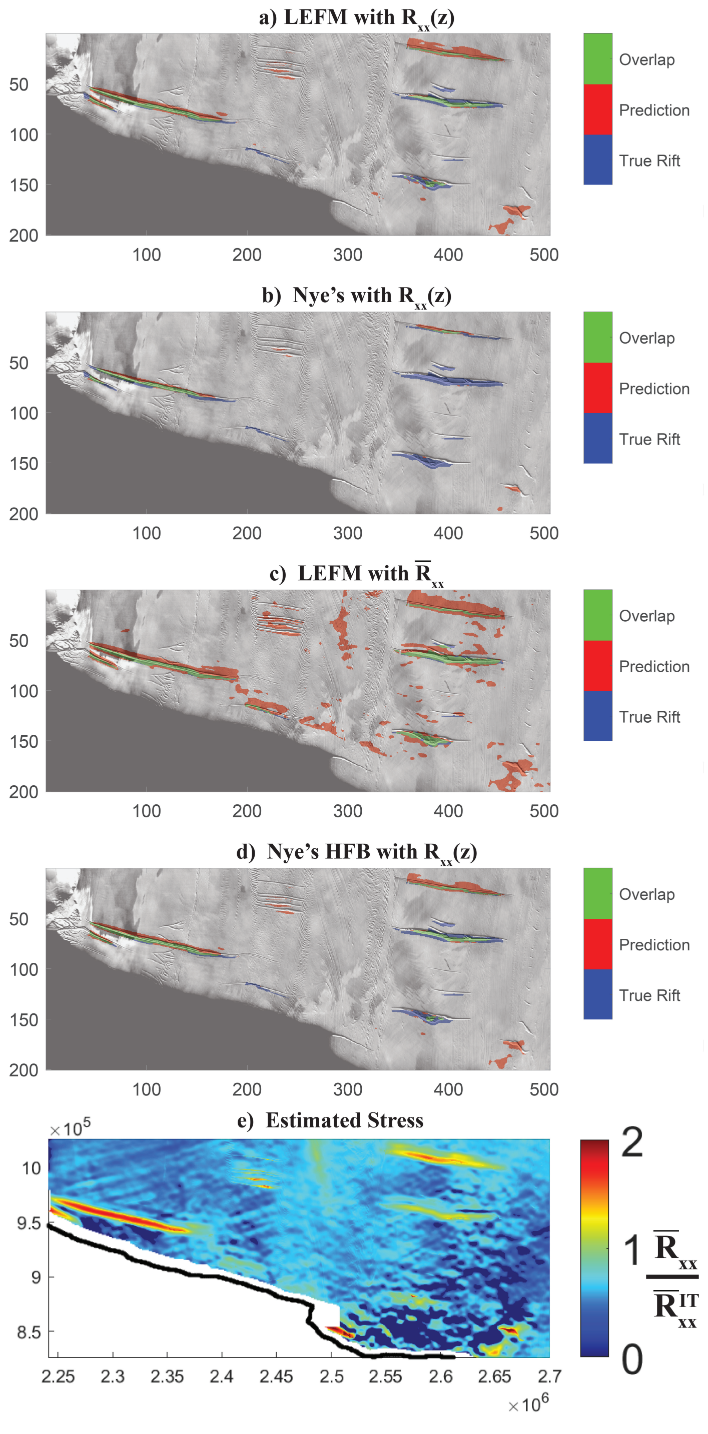

Figure 3. a) to d) are map views in kilometers of observed ((Walker et al., 2013); labeled as true rifts in blue) and theoretically predicted rifts (red) on the Ross Ice Shelf, overlain on MODIS MOA 2014 (Haran et al., 2018; Scambos et al., 2007), with correctly predicted rifts in green. Rift formation theories are a) LEFM with depth-varying stress due to temperature variation $R_{xx}(z)$, b) Nye's with $R_{xx}(z)$, c) LEFM with depth-averaged stress $\overline{R}_{xx}$, and d) Nye's with Horizontal Force Balance with $R_{xx}(z)$. e) is the estimated stress used for panel (a-d), with axes in meters. Known rifts are padded with locally unbroken ice thickness.

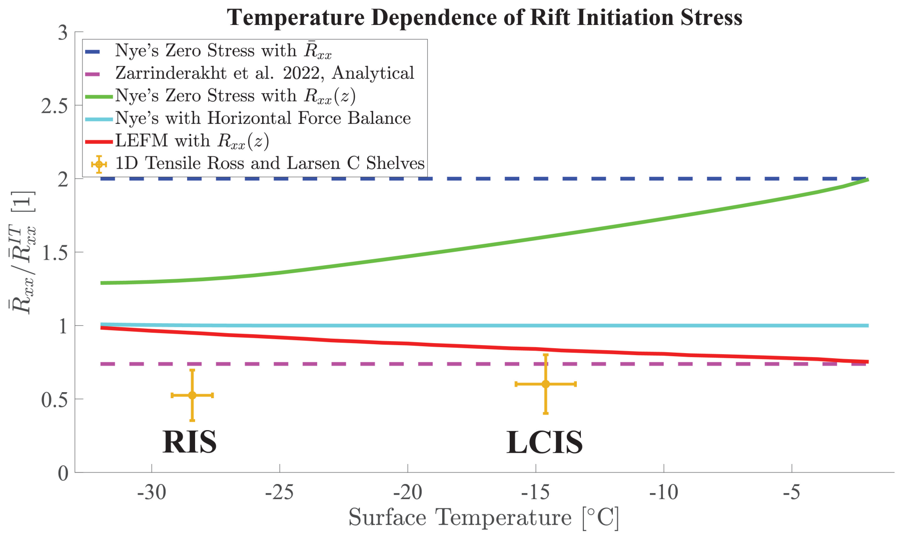

Figure 4. Nondimensional resistive stress required to initiate rifts versus surface temperature. The solid lines account for vertically-varying temperature structure through depth-varying stress $R_{xx}(z)$, whereas the dashed lines utilize depth-averaged resistive stress $\overline{R}_{xx}$. For a given theory, the region above and below the curve are predicted as a rift and non-rift, respectively. Extensional ice shelf data that is not rifted and upholds the 1D fracture assumptions is plotted in orange with mean and standard deviation. This data is shown in map view in Figure S4. We use the average thickness in the unbroken area surrounding the rifts as H to calculate $\overline{R}_{xx}^{IT}$. In this figure, surface temperatures colder than -25°C are on the Ross Ice Shelf (RIS), whereas those warmer are on the Larsen C Ice Shelf (LCIS). While the (Zarrinderakht et al., 2022) line in dashed magenta looks compelling with the intact ice shelf data in orange, map view analyses (see Figures 3c), S3c)) show that it overpredicts rifts.